Int. Conference on Boundary and Interior Layers
BAIL 2006
G.Lube, G.Rapin (Eds)

Turbulence Flow for NACA 4412 in Unbounded Flow and Ground Effect with Different Turbulence Models and Two Ground Conditions: Fixed and Moving Ground Conditions

A. Firooz[1], M. Gadami[2]

Mechanical Engineering Department,
University of Sistan & Baloochestan, Postal Code: 98164-161,
Daneshgah Avenue, Zahean, Iran
[1]E-mail: ahfirooz@hamoon.usb.ac.ir
[2]E-mail: gadami@mail.usb.ac.ir

Abstract

In this paper, the turbulence fluid flow ($Re = 2 \times 10^6$) around a two dimensional wing, NACA4412, on different angles of attack near and far from the ground for fixed and moving ground conditions with the RANS (Reynolds averaged Navier-stokes) equations is calculated. Realizable $K-\varepsilon$ turbulence model with Enhanced wall treatment and Spalart-Allmaras model are used. In order to validate the present numerical data the computational results for NACA 4412 in unbounded flow is compared with experimental data. The lift coefficient simulated by the moving bottom condition near the ground is greater than the fixed bottom condition, and far from the ground is vice versa, but the drag coefficient simulated by the moving bottom far from the ground is to some extent larger than that of the fixed one and near the ground is vice versa. Also it is concluded that on different angles of attack, lift coefficient of the airfoil, increases as it approaches the ground. In the moving ground condition the drag coefficient decreases as it approaches the ground, but in the fixed ground condition although the drag coefficient decreases far from the ground but it increases near the ground, as the airfoil approaches the ground.

1. Intruduction

Ever since the beginning of manned flight pilots have experienced something strange when landing an aircraft. Just before touch down it suddenly feels like the aircraft just does not want to go lower. It just wants to go on and on due to the air that is trapped between the wing and the runway, forming an air cushion. The air cushion is best felt in low wing aircraft with large wing areas. This phenomenon is called (aerodynamic) ground effect.

Two phenomena are involved when a wing approaches the ground. Ground effect is one name for both effects which is sometimes confusing. These two phenomena are a reduction of induced drag (D) and the latter in an increase of lift (L).

Very close to the ground, what is happening in reality is that the ground partially blocks the trailing vortices and decreases the amount of downwash generated by the wing. This reduction in downwash increases the effective angle of attack of the wing. The effect of this behavior is to increase the lift of wing. This phenomenon is what we call ground effect, "Stinton et al. [1]".

The aerodynamic characteristic of an airfoil in ground proximity is known to be much different from that of unbounded flow. The condition of the wind tunnel bottom, I. e., moving or fixed relative to the airfoil would influence the performance of the airfoil in ground effect. The presence of

boundary layer when air is flowing over bottom of the wind tunnel would be different from the real situation for a flying WIG, "Carr & Atkin et al. [2]". Proper velocity with the moving ground condition is considered, and boundary layer is considered with the fixed ground, and in the moving ground the boundary layer's effect is omitted, and so is the proper velocity in the fixed ground," Chang et al. [3]".

In this paper, turbulent flows around two-dimensional wing in ground effect are analyzed with incompressible Reynolds Averaged Navier-Stokes (RANS) equations which are approximated by finite volume method. The main object of this paper is to clarify the two-dimensional ground effect and it's flow characteristics due to different ground conditions, i.e., moving and fixed ground conditions, at different angles of attack with two turbulence models. Realizable K-ε turbulence model with Enhanced wall treatment and Spalart-Allmaras model are used.

First, in order to validate the present numerical data, the computational result of NACA 4412 ($\mathrm{Re} = 2\times10^6$) in unbounded flow at different angles of attack is compared with experimental data. Then NACA4412 pressure and velocity fields ($\mathrm{Re} = 2\times10^6$) are calculated for various ground clearances with two turbulence models and two ground conditions.

2. Governing equations

The governing equations for the turbulent incompressible flow encountered in this research are the steady-state Reynolds-averaged Navier-Stokes (RANS) equations. The turbulent viscosity is computed through two different turbulence models, Realizable $k-\varepsilon$ turbulence model, "Litchford, Jeng et al. [4]", and Spalart and Allmaras turbulence model, "Merz, Kruckels, Mayer, Stetter et al. [5]", Equations are approximated by finite volume method, and they are solved by segregated method. The second order upwind method, "Barth, Jespersen et al. [6]", is used for the convection term, also for pressure interpolation the PRESTO, "Patankar et al. [7]", method is used, and the relation between pressure and velocity with SIMPLEC algorithm, "Vandoormaal, Raithby et al. [8]", is calculated.

3. Wall treatment

The application of wall functions to modeling the near-wall region may significantly reduce both the processing and storage requirements of a numerical model, while producing an acceptable degree of accuracy. The non-dimensional wall parameter is defined as:

$$y^+ = \frac{\rho\sqrt{\frac{\tau_w}{\rho_w}}y_p}{\mu} \qquad (1)$$

In "Eq. (1)", y_p is the distance from the first computational node to the wall and the subscript w denotes wall properties, "Speziale, Abid, Anderson et al. [9]". Enhanced wall treatment is a method of near-wall modelling that utilizes the combination of a two-layer zonal model, "Gresho, Lee, Sani et al. [10]" with enhanced wall functions.

4. Computational domain and mesh generation

The computational domain extended 3C upstream of the leading edge of the airfoil, 5C downstream of the trailing edge, and 4C above the pressure surface. Distance of below the airfoil was defined with H/C where C is chord, and H is ground distance at the trailing edge.

Velocity inlet boundary condition was applied upstream (Inflow) with speed of (U_∞=29.215) and outflow boundary condition was applied downstream. The pressure and suction side of the airfoil and above and below' s boundaries of domain were defined independently with no slip wall boundary condition. Moving wall with speed of (U_∞=29.215) for above (far flow), and fixed or moving wall for below (Ground) the airfoil were used, "Figure 1", Nicholas, at al. [11]".

An unstructured mesh arrangement with quadrilateral elements was adopted to map the flow domain in ground effect. Particular attention was directed to an offset 'inner region' encompassing the airfoil, and also C-type mesh was applied on near the airfoil at above and bottom, which it's domain depends on the H/C in ground effects condition. A considerably fine C-type mesh was applied to achieve sufficient resolution of the airfoil surface and boundary layer region. Continuing downstream from leading edge and continuing far from above the airfoil H-type mesh was applied.

By increasing the grid numbers and changing the type of arranging mesh, refining, around the airfoil a proper y^+ value is obtained, and with this value solution results have good agreement with experimental data, "Abbott, Doenhoff et al. [12], "Figures 2 to 3".

5. Computational results & discussion

A grid independence analysis was conducted using seven meshes of varying cell number. Each mesh was processed using the Realizable $k-\varepsilon$ turbulence model with Enhanced wall treatment and Spalart-Allmaras model, at a free-stream velocity of 29.215m/s ($\mathrm{Re} = 2\times10^6$). "Table (1)" shows the node and y^+ characteristics of each mesh.

Mesh G and F achieve considerably low average y^+ value, sufficiently resolving the laminar sublayer (i.e $y^+ \leq$ 4-5). The maximum and average value of mesh E, and D indicate that its resolution extends to buffer layer (i.e $5 \leq y^+ \leq 30$). Mesh A shows significant coarseness with considerably large maximum and minimum y^+ value, indicating resolution to turbulent outer layer (i.e $y^+ \geq 30$). The maximum y^+ value of mesh B and C is resolved in turbulent outer and its minimum y^+ value is resolved in buffer layer.

"Table 2" shows predicted lift and drag coefficients with Spalar-Almaras model at $\alpha = 6$ and also it is computed for different angles of attack and compared with experimental data, "Abbott, Doenhoff et al. [12], in "Figure 4". It can be concluded that by using of mesh F and G predicting almost identical coefficients and have good agreement with experimental data. In this suggestion, grid independence has been achieved. If the resolution extends to buffer layer, the numerical data have not good agreement with experimental data.

"Table 3." shows predicted lift and drag coefficients with Realizable $K-\varepsilon$ turbulence model at $\alpha = 6$ and also it is computed for different angles of attack and compared with experimental data in "Figure 5". Lift coefficient predicted by using of mesh refinement for this model doesn't have clear difference, except mesh A that indicate a little difference.

"Figure 6" shows Cp variation on surface of the airfoil at seven relative ground height computed for two ground conditions ($\alpha = 6^o$, $\mathrm{Re} = 2 * 10^6$). By comparing the pressure fields in unbounded flow and ground effect, it can be noticed that a dramatic pressure increases in the region between the lower surface of the airfoil and the ground occurs, resulting in the lift increase. As the airfoil approaches the

ground, the pressure on the pressure side of wing gradually increases due to slow-down of flow, "Chun, Chang at al. [13]", (Figures 8 to 9), although the pressure on the suction side of airfoil gradually increases, but the increase rate of the pressure on the pressure side is much larger than that of suction side, resulting in lift increase that is regarded as the advantage of the WIG vehicle.

The velocity fields around NACA 4412 in unbounded flow ($\alpha = 6^o$, $Re = 2 * 10^6$) are shown in "Figure 7". The velocity fields around this section in ground effect with H/C=0.08 for two different ground conditions at $\alpha = 6$ are shown in "Figure 8 to 9". The difference in the velocity field near the airfoil surface due to the different bottom conditions and a boundary layer developed on the fixed ground can be clearly seen. On the other hand, for the moving ground with oncoming undisturbed velocity as seen in "Figure 8", the velocity decreases with increasing height. The results for three grounds heights of H/C=0.08, 0.1, 0.2, are redrawn in "Figure 10". By comparison cp variation for two different ground conditions, it can be seen that the pressure difference between fixed and moving ground on the pressure side of the airfoil increases as the H/C decreases. In fact cp under about of H/C=0.2 in the pressure side for the fixed ground is lower than the moving one, resulting in large decrease lift for the fixed ground condition as is mentioned later in "Figure13 ", and also cp in the suction side near to the leading edge gradually increases as H/C decreases. This can be attributed to the fact that for an airfoil in ground effect, some of the slow-down flow entrapped in between the underside of the airfoil and the ground, has escaped over the airfoil. Due to the boundary developed on the fixed ground, escape flux over the airfoil for the fixed ground is larger than that of the moving one and so cp increases near the leading edge in the suction side for the fixed ground more than that of moving one, resulting in pressure drag coefficient increase for the fixed ground condition as is mentioned later in "Figure 15".

"Figure 11" shows C_L at different ground clearances for different angles of attack. It can be seen C_L increases with decreasing H/C and increasing angles of attack.

"Figure 12" shows C_D at different ground clearances for different angles of attack. It can be seen C_D increases with increasing H/C and increasing angles of attack.

"Figure 13" shows C_L at different ground clearances for different angles of attack, for two ground conditions. As mentioned before by comparison between fixed and moving ground C_L largely decreases at the certain distance (h/c) in the fixed ground, this distance increases as the angel of attack increases, as shown in "Figure 14". The "h" is the distance in which escape flux and influence of boundary layer occurs in the fixed ground condition and because of this the variation of C_L in fixed and moving ground differs. Also "Figure 13" shows C_L in the fixed ground far from the ground, due to boundary layer region in ground, in which velocity decreases, in some extent larger than the moving ground condition. Also it is concluded that on different angles of attack lift coefficient of the airfoil increases as it approaches the ground.

"Figure 15" shows C_D at different ground clearances for different angles of attack, for two ground conditions. Due to the escape flux for the fixed ground Cp increases in the suction side of the airfoil, and C_f increases due to velocity gradient increasing in pressure side resulting a largely increase C_D for the fixed ground condition. In the moving ground, on different angles of attack, the drag coefficient decreases as the airfoil approaches the ground, and in fixed ground the drag coefficient decreases far from the ground and increases near the ground, as it approaches the ground.

"Table 4" shows lift & drag & pressure drag & friction drag coefficients at different ground clearances and different ground conditions with Spalart-Allmaras turbulence model at $\alpha = 6$. It can be seen that C_f decreases as H/C decreases for both moving and fixed ground, which may be attributed to the fact that the velocity gradient on the pressure side of the airfoil becomes smaller by flow slow-down with approaching the ground. It is noticed that the difference in C_f for two ground conditions

above about of H/C=0.2 seems to be negligible. However, a dramatic change in Cp by two ground conditions can be noticed.

Results of performance of each model are presented with respect to the predicted lift and drag coefficients at different ground clearances. It can be seen the Realizable $K-\varepsilon$ turbulence model and Spalart-Allmaras model almost predict identical lift coefficients (Figure 16). But "Figure 17" shows clear difference between predicted drag coefficients by use of these models.

6. Conclusion

The flow characteristics for two-dimensional wings in ground proximity are analyzed with RANS equations, and approximated by finite volume schemes, with Spalart-Allmaras and Realizable $K-\varepsilon$ turbulence models. The difference in the flow characteristics due to two ground conditions is examined for NACA4412. Based on this study, some conclusions can be drawn as:

- A grid independence analysis was conducted using seven meshes of varying cell number. Each mesh was processed using the Realisable $K-\varepsilon$ turbulence model with Enhanced wall treatment and Spalart-Allmaras model. For Spalart-Allmaras model if the resolution extends to viscous sublayer, the numerical data have good agreement with experimental data. In this suggestion, grid independence has been achieved. If the resolution extends to buffer layer, the numerical data have not good agreement with experimental data.
- As airfoil approaches the ground, the pressure on the pressure side of the airfoil gradually increases due to the slow-down of the flow, resulting in a large lift increase.
- It can be clearly seen that a relatively thick boundary on the fixed ground is developed, compared to the moving ground. Due to this fact, the flow characteristic of an airfoil with two ground conditions, near and far from the ground would be different. Due to the boundary layer developed on the fixed ground, velocity increases in pressure side and pressure decreases in this region and also some of the slow-down flow entrapped in between the under side of the airfoil and ground, has escaped over the airfoil for the fixed one, and so pressure increases near to the leading edge for suction side, resulting lift simulated by the moving bottom condition near the ground is greater than the fixed bottom condition and far from the ground is vice versa.
- For the fixed ground condition, due to the escape flux near the ground, pressure drag coefficient increases in suction side, also velocity gradient increases in pressure side resulting friction drag coefficient increases, so drag coefficient simulated by the fixed ground near the ground, is to some extent larger than that of the fixed one.
- It is concluded that on different angles of attack lift coefficient of the airfoil increases as it approaches the ground. In the moving ground condition the drag coefficient decreases as it approaches the ground, but in the fixed ground condition although the drag coefficient decreases far from the ground but it increases near the ground, as the airfoil approaches the ground, but in the fixed ground condition although the drag coefficient decreases far from the ground but it increases near the ground, as the airfoil approaches the ground.

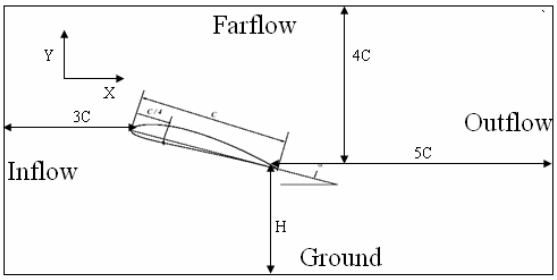

Figure1. The dimensions and boundary conditions of the computational domain

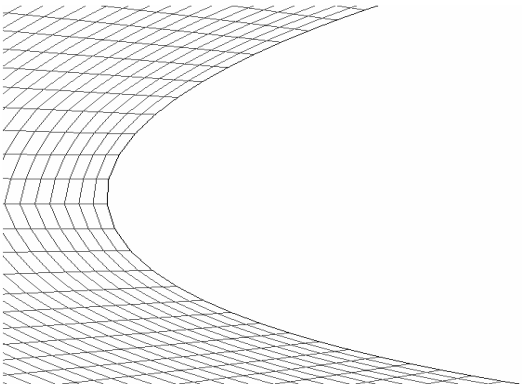

Figure 2. Zoom of C-grid around leading edge

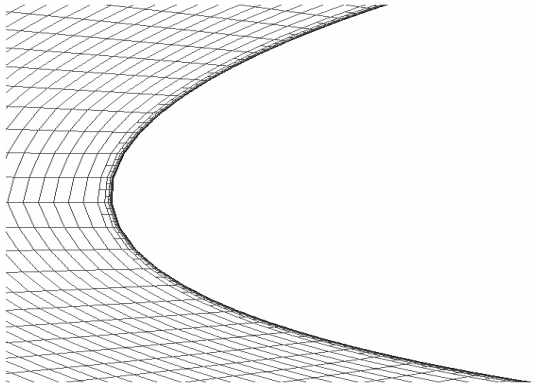

Figure 3. Zoom of refined C-grid around leading edge

Table 1. Grid Independence Analysis- Mesh node and y^+ characteristics

mesh	*Node*	*Y+*	
		max	*min*
A	181202	200	80
B	182411	90	20
C	184816	50	10
D	189628	28	7.5
E	199241	16	1
F	218458	9	0.5
G	256875	5	0.2

Table 2. Grid Independence Analysis-lift & drag coefficients with Spalar-Allmaras Turbulence model ($\alpha = 6^o$, $Re = 2*10^6$)

mesh	C_L	C_D
A	1.1106	0.018039
B	1.0963	0.017833
C	1.1158	0.01734
D	1.1153	0.016301
E	1.107	0.016603
F	1.09	0.01785
G	1.0848	0.01815

Table 3. Grid Independence Analysis-lift & drag coefficients with $K-\varepsilon$ Turbulence model ($\alpha = 6^o$, $Re = 2*10^6$)

mesh	C_L	C_D
A	1.128	0.01812
B	1.1	0.018782
C	1.095	0.018277
D	1.0933	0.017577
E	1.0925	0.017816
F	1.092	0.018001
G	1.0972	0.017616

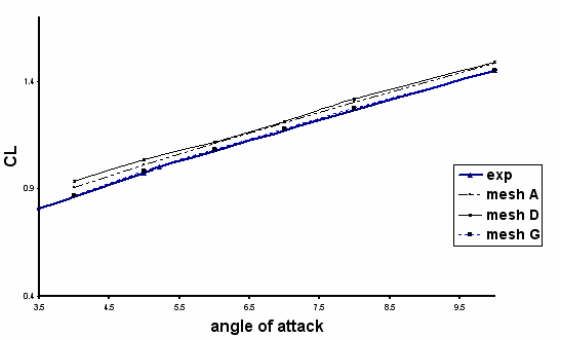

Figure 4. C_L vs. angle of attack with Spalllar-Allmaras turbulence Model

Experimental data (Abbott, Doenhoff et al. [12]).

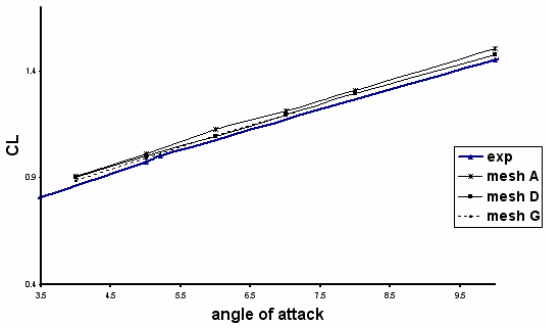

Figure 5. C_L vs. angle of attack with $K-\varepsilon$ turbulence model

Experimental data (Abbott, Doenhoff et al. [12]).

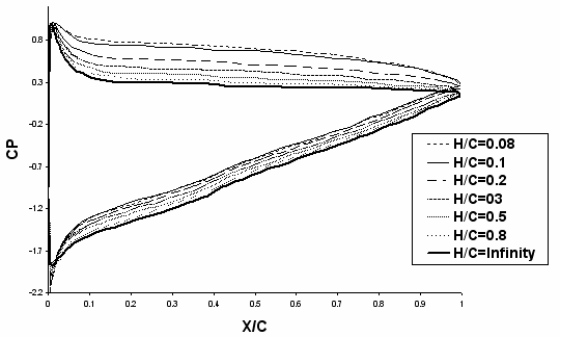

Figure 6. Surface pressure distributions for NACA 4412 at different ground clearances in Moving ground (α =6^o, Re = 2 *10^6)

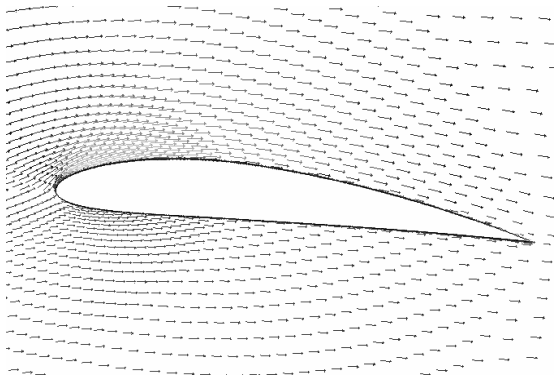

Figure 7. Velocity vector for NACA 4411 in unbounded flow (α =6^o, Re = 2 *10^6)

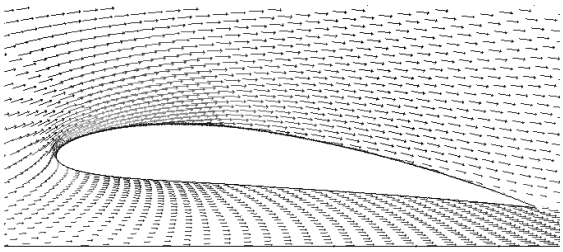

Figure 8. Velocity vector for NACA 4412 in ground effect (α =6^o, Re = 2 *10^6, H/C=0.08, Moving ground)

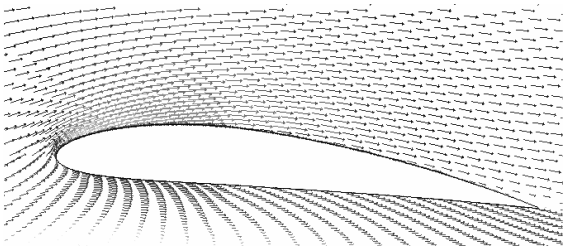

Figure 9. Velocity vector field for NACA 4412 in ground effect (α =6^o, Re = 2 *10^6, H/C=0.08, Fixed ground)

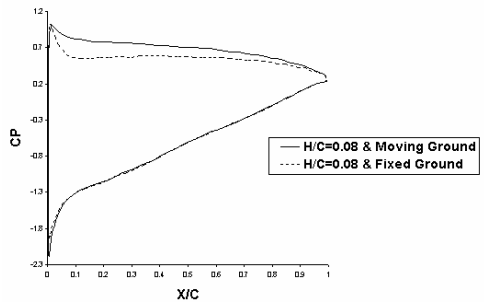

Figure 10. a. (H/C=0.08)

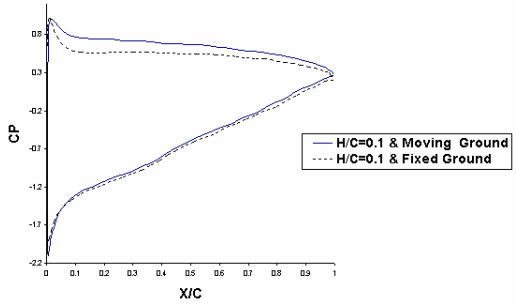

Figure 10.b. (H/C=0.1)

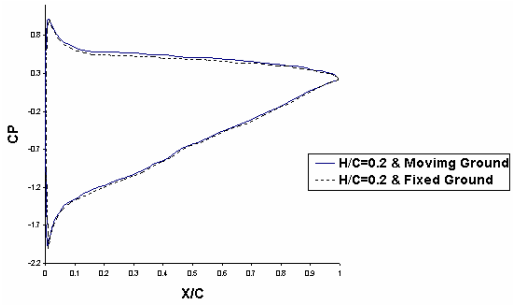

Figure 10.c. (H/C=0.2)

Figure 10. Surface pressure distributions for NACA 4412 in ground effect with two ground conditions ($\alpha = 6^o$, Re = 2 *10^6)

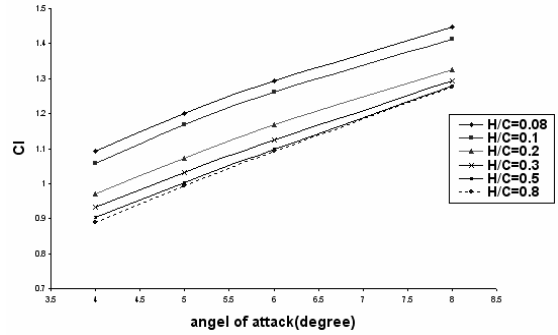

Figure 11. Variation of C_L vs. angel of attack for NACA 4412 at different ground clearances in Moving ground (Re=2*10^6)

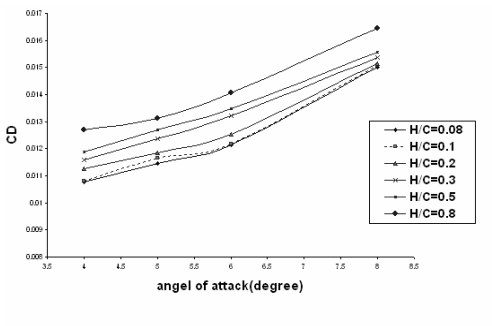

Figure 12. Variation of C_D vs. angel of attack (degree) for NACA 4412 at different ground clearances in Moving ground (Re=2*10^6)

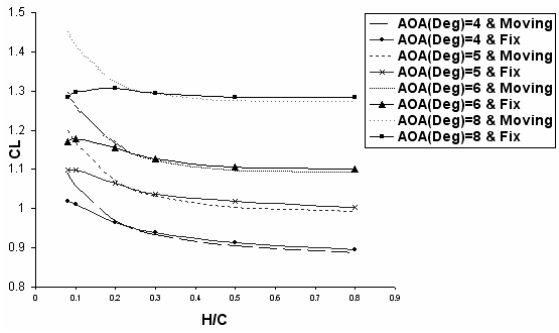

Figure 13 .Variation of C_L vs. H/C for NACA 4412 at different angles of attack and at different ground clearances with two ground conditions (Re=2*10^6)

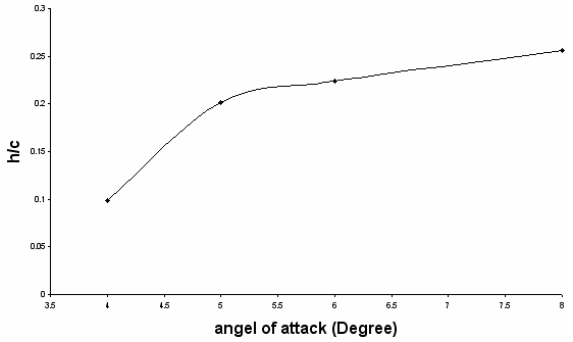

Figure 14. Variation of h/c vs angel of attack for NACA 4412

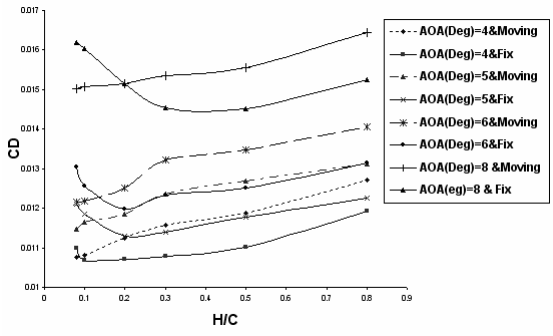

Figure 15. Variation of C_D vs. H/C for NACA 4412 at different angles of attack and at different ground clearances with two ground conditions ($Re=2*10^6$)

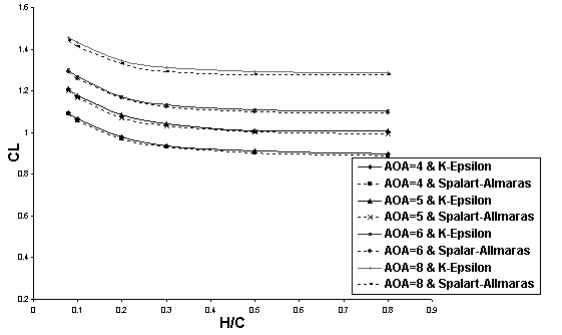

Figure 16. Variation of C_L vs. H/C for NACA 4412 at different angles of attack and at different ground clearances with two turbulence models in Moving ground ($Re=2*10^6$)

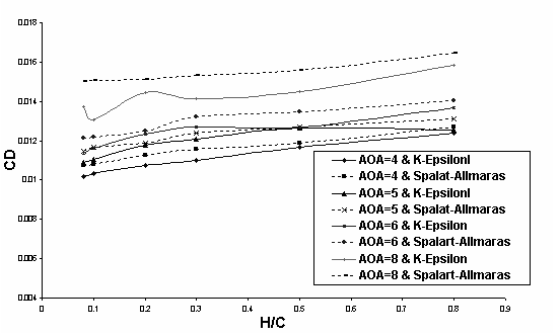

Figure 17. Variation of C_D vs. H/C for NACA 4412 at different angles of attack and at different ground clearances with two turbulence models in Moving ground ($Re=2*10^6$)

Table 4. Lift & Drag & Pressure drag & friction drag coefficient at difference ground clearances with two ground conditions with Spalat-Allmaras turbulence model ($\alpha=6^o$, $Re = 2*10^6$)

H/C	*CL*		*CD*10*		*Cf*100*		*Cp*100*	
	moving	*fixed*	*moving*	*fixed*	*moving*	*fixed*	*moving*	*fixed*
0.08	1.2934	1.171	0.12144	0.1304	0.61594	0.6889	0.59843	0.61514
0.1	1.2603	1.1791	0.1219	0.12566	0.63744	0.6855	0.58183	0.57097
0.2	1.1674	1.156	0.12518	0.11969	0.7022	0.7167	0.5495	0.48012
0.3	1.1241	1.1271	0.13209	0.12344	0.75362	0.7619	0.56723	0.4722
0.5	1.0975	1.1064	0.13474	0.12518	0.78268	0.7877	0.5952	0.464
0.8	1.093	1.1017	0.14052	0.13139	0.807	0.80766	0.60022	0.50685
∞	1.0848		0.1815		0. 8576		0.9575	

REFERENCES

1) D. Stinton, "The Anatomy of the Aeroplan", 2nd Edition published Blacewell Science, pp. 86-92 (1998).

2) G. W. Carr and P. D. Atkin, "influence of Moving Belt Dimension on Vehicle Aerodynamic Force", Proc. of Wind Tunnels and Wind Tunnel Test Techniques, Published by The Royal Aernautical Society, London, pp.37.1-37.16 (1997).

3) R. H. Chang, "Numerical Simulation of Turbulent Flow around Two-Dimensional Wings In Ground Effect Wing Different Ground Boundary Condition", MSc Thesis, Dept of Naval Architecture & ocean Engineering Pusan National University, Korea72 (2000).

4) R. J. Litchford and M. S Jeng,, "Efficient Statistical Transport Model for Turbulent Particle Dispersion in Sprays". AIAA Journal, 29:1443 (1991).

5) R. Merz and J. Kruckels and J. Mayer, and H. Stetter, "Computation of Three Dimensional Viscous Transonic Turbine Stage Flow Including Tip Clearance Effiects", ASME *95-GT-76* (1995).

6) T. J. Barth and D. Jespersen, "The design and application of upwind schemes on unstructured meshes", Technical Report AIAA- 89-0366, AIAA 27th Aerospace Sciences Meeting, Reno, Nevada (1989).

7) S. V. Patankar, "Numerical Heat Transfer and Fluid Flow", Hemisphere, Washington, D.C (1980).

8) J. P. Vandoormaal, and G. D. Raithby, "Enhancements of the SIMPLE Method for Predicting Incompressible Fluid Flows", Numer Heat Transfer, 7:147{163} (1984).

9) C.G. Speziale and R. Abid and E.C. Anderson, "Critical Evaluation of Two-Equation Models for Near-Wall Turbulence", AIAA J., Vol. 30 No. 2, pp. 324-331(1992).

10) P. M. Gresho and R. L. Lee and R. L. Sani, "On the Time-Dependent Solution of the Incompressible Navier-Stokes Equations in Two and Three Dimensions", In Recent Advances in Numerical Methods in Fluids, Pineridge Press, Swansea, U.K (1980).

11) Nicholas and J. Mulvany and Li Chen and JiYuan Tu and Brendon Anderson "Steady-State Evaluation of 'Two-Equation' RANS (Reynolds-averaged Navier-Stokes) Turbulence Models for High-Reynolds Number Hydrodynamic Flow Simulations" , DSTO Platform Sciences Laboratory Commonwealth of Australia 2004 AR-013-055 (2004).

12) I.H. Abbott and A.E .von Doenhoff, "Theory of Wing Sections", Dover, New York (1959).

13) H.H. Chun and R. H. Chang " Turbulence flow Simulation for Wings in Ground Effect with Two Ground Condition Fixed and Moving Ground", International Journal of Maritime Engineering (2003).